6th European Conference on Computational Mechanics (ECCM 6)
7th European Conference on Computational Fluid Dynamics (ECFD 7)
11-15 June 2018, Glasgow, UK

EFFECT OF HUMPS AND INDENTATIONS ON BOUNDARY-LAYER TRANSITION OF COMPRESSIBLE FLOWS USING THE AHLNS METHODOLOGY

J. A. Franco[1], S. Hein[2] and E. Valero[3]

[1] German Aerospace Center (DLR), Institute of Aerodynamics and Flow Technology, 37073 Goettingen, Germany, Juan.Franco@dlr.de

[2] German Aerospace Center (DLR), Institute of Aerodynamics and Flow Technology, 37073 Goettingen, Germany, Stefan.Hein@dlr.de

[3] Universidad Politécnica de Madrid (UPM), ETSIAE-UPM (School of Aeronautics), 28040 Madrid, Spain, Eusebio.Valero@upm.es

Key words: Laminar-Turbulent Transition, Surface Irregularities, Stability, AHLNS

Abstract. The presence of surface irregularities like humps or indentations can cause regions of localized strong streamwise gradients in the basic flow quantities. These large gradients can significantly modify the linear mechanisms that lead to laminar-turbulent transition in wall-bounded flows (e.g. Tollmien-Schlichting waves). Standard methodologies like LST (Local Stability Theory) or PSE (Parabolized Stability Equations) can be applied in regions far from the surface irregularities where the streamwise variations are small. However, their formulations are not suited for handling the presence of such large streamwise gradients.

The Adaptive Harmonic Linearized Navier-Stokes (AHLNS) equations can handle these large streamwise gradients by using a fully-elliptic system of equations as in DNS (Direct Numerical Simulation). Moreover, as in PSE a wave-like character of the instabilities is assumed, leading to a significant reduction in the number of streamwise grid points required compared with DNS computations.

In the present study, smooth humps/indentations with height/depth comparable with the local boundary-layer displacement thickness are investigated. The effect of the hump/indentation on the spatial evolution of convective instabilities, in terms of N-factors, is presented. It is shown that the shape of the surface irregularity plays an important role in the growth of convective instabilities.

1 INTRODUCTION

Local stability theory (LST) and parabolized stability equations (PSE) equations have been successfully applied to study the development of convective instabilities (e.g. Tollmien-Schlichting (TS) waves) in boundary-layer flows and, based on the e^N methodology, to

provide a reasonable transition location. However, the presence of surface irregularities such as steps, humps, gaps, etc. may interact with the incoming disturbance in such a way that neither of these methodologies is able to reproduce the growth of the instabilities correctly. In the PSE approach it is assumed that the streamwise variation of the laminar basic flow and of the disturbance properties are small over the characteristic wavelength of the instability mode. In the LST method such streamwise gradients are neglected at all. However, the presence of the surface irregularities can cause regions of localized strong streamwise flow gradients.

The Adaptive Harmonic Linearized Navier-Stokes (AHLNS) formulation used here is derived from the PSE approach by removing the assumption in PSE of a 'slowly varying flow in streamwise direction'. This assumption is abandoned by recovering all terms dropped in the original PSE formulation excluded during the parabolization process. As opposed to the PSE formulation, in the AHLNS formulation there is no restriction regarding all streamwise variations of geometry, mean flow and disturbance flow. PSE is solved by a marching procedure. However, some remaining ellipticity in the equations restricts the minimum step size. In the AHLNS approach, no marching procedure is used to solve the governing equations. This allows the use of an arbitrarily fine grid in regions of strong streamwise flow gradients.

The effect of humps/indentations in the laminar-turbulent transition process have been extensively studied in the literature. Nenni & Guyas [8] focused on finding a critical height/depth. Woerner *et al.* [9] studied the influence of the height and width of rectangular humps for an incompressible flow. They concluded that the height of the hump was the most important geometrical parameter in terms of amplification of TS waves. A similar conclusion was provided by Franco & Hein [2] when they investigated rectangular humps based on the set-up of Dovgal *et al.* [10]. A study considering smooth humps was done by Park & Park [11] using PSE. However, the hump heights analyzed in their work were relatively small compared with the local boundary-layer displacement thickness δ_1. Garicano *et al.* [1] examined several indentations with depths comparable to δ_1 using a biglobal temporal approach. In the present paper, we are interested in the study of the effect of the shape of humps/indentations on the spatial evolution of convective instabilities in the compressible regime when the height/depth of the hump/indentation is comparable to δ_1.

2 AHLNS EQUATIONS

Here, a brief introduction to the Adaptive Harmonic Linearized Navier Stokes (AHLNS) equations is given. For a detailed description of the methodology, the readers are referred to Franco & Hein [2] and Guo *et al.* [3].

2.1 Governing equations

The AHLNS equations are obtained from the compressible Navier-Stokes (NS) equations linearized for small disturbances. All flow and material quantities are decomposed into a steady basic flow $\bar{\mathbf{q}}$ plus an unsteady disturbance flow component $\tilde{\mathbf{q}}$, i.e.

$$\mathbf{q}(\mathbf{x},t) = \bar{\mathbf{q}}(\mathbf{x}) + \varepsilon\tilde{\mathbf{q}}(\mathbf{x},t), \quad \varepsilon \ll 1, \tag{1}$$

where x, y and z are the streamwise, spanwise and normal coordinate components of the position vector $\mathbf{x}$. Here, t represents time. This flow decomposition is introduced into the NS equations, then the basic state solution is subtracted and products of disturbance quantities are neglected. To further simplify the analysis, it is assumed that the basic flow is independent of the y coordinate, while the disturbance flow is periodic in the y-coordinate, i.e. the analysis is restricted to quasi-three dimensional flows. The adaptive approach proposed by Guo *et al.* [3] is introduced here: the disturbance flow variables are divided into an amplitude function and an oscillating or wave function, i.e.

$$\tilde{\mathbf{q}}(x,y,z,t) = \hat{\mathbf{q}}(x,z)e^{i\Theta}, \tag{2}$$

where the wave function is defined as

$$\Theta = \int \alpha(x)dx + \beta y - \omega t. \tag{3}$$

The physical disturbance is recovered from the real part of $\tilde{\mathbf{q}}$. Once these assumptions are introduced into the NS equations, the AHLNS equations are obtained. They can be written in matrix form

$$\mathbf{A}\hat{\mathbf{q}} + \mathbf{B}\frac{\partial\hat{\mathbf{q}}}{\partial z} + \mathbf{C}\frac{\partial^2\hat{\mathbf{q}}}{(\partial z)^2} + \mathbf{D}\frac{\partial\hat{\mathbf{q}}}{\partial x} + \mathbf{E}\frac{\partial^2\hat{\mathbf{q}}}{\partial x\partial z} + \mathbf{F}\frac{\partial^2\hat{\mathbf{q}}}{(\partial x)^2} = 0, \tag{4}$$

where $\hat{\mathbf{q}} = (\hat{\rho},\hat{u},\hat{v},\hat{w},\hat{T})^\top$. Here, ρ and T stand for density and temperature, while u, v, w are the streamwise, spanwise and normal components of the velocity vector $\mathbf{u}$. The coefficients $\mathbf{A}-\mathbf{F}$ are 5×5 matrices, which contain basic flow quantities, real-valued parameters β and ω, and the complex-valued wavenumber α. The disturbance field is subjected to the following boundary conditions

$$\begin{aligned} \hat{u} = \hat{v} = \hat{w} = \hat{T} = 0 \quad at \quad z = 0 \\ \hat{u} = \hat{v} = \hat{w} = \hat{T} = \hat{\rho} \to 0 \quad as \quad z \to \infty. \end{aligned} \tag{5}$$

Once the boundary conditions are incorporated into the system of equations, Eqn. (4), and after discretization, a system of linear algebraic equations of the form $\mathbf{L}\hat{\mathbf{q}} = \mathbf{b}$ is reached, where vector $\mathbf{b}$ collects the information of the inflow boundary condition.

In the adaptive approach, similar to the PSE approach, a first result for $\hat{\mathbf{q}}$ is obtained for a given initial distribution of $\alpha(x)$. Then a new distribution of $\alpha(x)$ can be computed from the solution that minimizes the streamwise variation of $\hat{\mathbf{q}}$. This new $\alpha(x)$ is again used to compute a new solution. The process is repeated until the solution converges. This iterative process is driven by a normalization condition already used in PSE:

$$\alpha_{new} = \alpha_{old} - i\frac{\int_0^\infty \left(\hat{u}^\dagger\frac{\partial\hat{u}}{\partial x} + \hat{v}^\dagger\frac{\partial\hat{v}}{\partial x} + \hat{w}^\dagger\frac{\partial\hat{w}}{\partial x} + \hat{T}^\dagger\frac{\partial\hat{T}}{\partial x} + \hat{\rho}^\dagger\frac{\partial\hat{\rho}}{\partial x}\right)dz}{\int_0^\infty \left(||\hat{u}||^2 + ||\hat{v}||^2 + ||\hat{w}||^2 + ||\hat{T}||^2 + ||\hat{\rho}||^2\right)dz}, \tag{6}$$

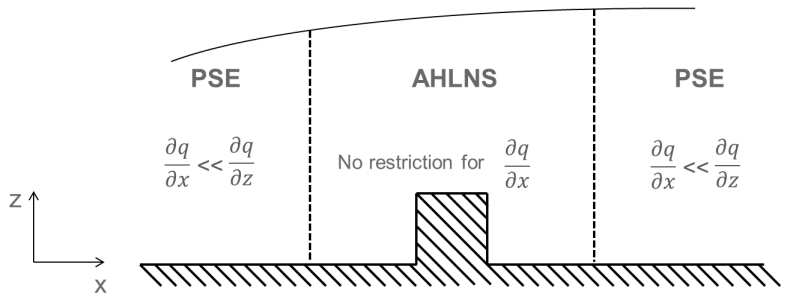

Figure 1: Sketch of the multi-zonal technique for boundary-layer instability analysis in the presence of surface irregularities. The vertical dashed lines represent the inflow and outflow locations for AHLNS computations. Magnitude q holds for both basic flow quantities $\bar{q}$ and amplitude function of the disturbances $\hat{q}$. Flow direction is from left to right.

with superscript † referring to the complex conjugate. This normalization condition minimizes the streamwise variation of the amplitude functions $\hat{\mathbf{q}}$. Therefore, the number of grid points in streamwise direction can often be reduced considerably compared with DNS. This is the basic idea behind the solution-adaptive scheme. A more detailed description of this iterative process can be found in the work of Franco & Hein [2] or Guo *et al.* [3].

2.2 Multi-zonal approach

Figure 1 illustrates a typical example of a wall-bounded flow with a local surface irregularity (in this case, the presence of a rectangular hump on a flat plate) and indicates where AHLNS is applied in a multi-zonal approach. Relatively far away from the surface irregularity, the streamwise variations of the laminar basic flow $\frac{\partial \bar{q}}{\partial x}$ and amplitude functions $\frac{\partial \hat{q}}{\partial x}$ are still relatively small and the assumptions made for PSE are valid. However, in the vicinity of the surface irregularity the streamwise gradients may be of the same order as the wall-normal gradients, and AHLNS is applied. At the inflow location of the AHLNS zone, the amplitude functions provided by PSE are taken as inflow boundary condition for AHLNS. At the outflow location of the AHLNS zone, the amplitude functions provided by AHLNS can be used as initial condition for a subsequent PSE computation. The inflow and outflow boundaries of the AHLNS domain are placed where the assumption of a slow streamwise variation of the laminar basic flow and of the amplitude functions is valid.

2.3 Growth rate and N-factor envelope

The physical growth rate σ of an arbitrary disturbance quantity ξ is defined as

$$\sigma_\xi = -\alpha_i + Real\left(\frac{1}{\xi}\frac{\partial \xi}{\partial x}\right), \tag{7}$$

where the first r.h.s term is the contribution of the exponential part of the disturbance. The second term is the correction due to changes of the amplitude function. In the present paper, ξ is taken to be the streamwise velocity component $\hat{u}$ at the normal location where $\hat{u}$ reaches its maximum value. The n-factor, which measures the accumulated growth of the disturbances, is computed as

$$n = \int_{x_s}^{x} \sigma_{\hat{u}} dx, \tag{8}$$

where x_s denotes the streamwise position where the disturbance starts to grow. Each n-factor curve is computed for a single frequency f. The envelope of these curves is called the N-factor envelope, following the definition given by Arnal [4].

3 RESULTS

3.1 Basic flow computations

The laminar steady two-dimensional flow on a flat plate in the presence of a hump/indentation has been computed numerically. The compressible Navier-Stokes (NS) solver TAU [5], developed at DLR, was used. Grids were generated using the structured grid generator MEGACADS, also developed at DLR. All geometrical parameters have been nondimensionalized using the incompressible boundary-layer displacement thickness δ^* at a certain x_0^* position from the leading edge, for which in the case of a flat plate flow at zero pressure gradient, takes the expression (see Schlichting [6])

$$\delta^* = 1.7208\sqrt{\left(\frac{\mu_\infty x_0^*}{\rho_\infty U_\infty}\right)}, \tag{9}$$

where μ_∞, ρ_∞ and U_∞ stand for the dynamic viscosity, density and velocity at the boundary-layer edge. In the rest of the paper, the non-dimensional x-coordinate will be referred to the x_0^* position, i.e.

$$x = \frac{x^* - x_0^*}{\delta^*}, \tag{10}$$

where x^* is the dimensional distance from the leading edge. The Reynolds number based on δ^* is defined as

$$Re_{\delta^*} = \frac{\rho_\infty U_\infty \delta^*}{\mu_\infty}, \tag{11}$$

and set to 610. The Mach number Ma_∞ is 0.5 for all computations. The shape of the humps and indentations is given by the expression

$$z = \pm D \exp\left(-\left(\frac{x - x_c}{L/2}\right)^{2m}\right), \quad \text{with} \quad m = 1, 2, 3, 4, \ldots, \tag{12}$$

where the parameter D indicates the height (+)/depth (-) of the hump/indentation, and parameter L its width. The center of the surface irregularity is placed at x_c. Since our investigations are focused on the effect of the shape of the surface irregularity, parameters D, L and x_c will be constant for all simulations with 1.5, 50 and 100, respectively. The geometrical parameter m will be varied from 1 to 4. In the case of an indentation, a sketch showing the wall shape is depicted in Figure 2 for several values of m (including the rectangular case, which can be considered the limiting case when $m \to \infty$).

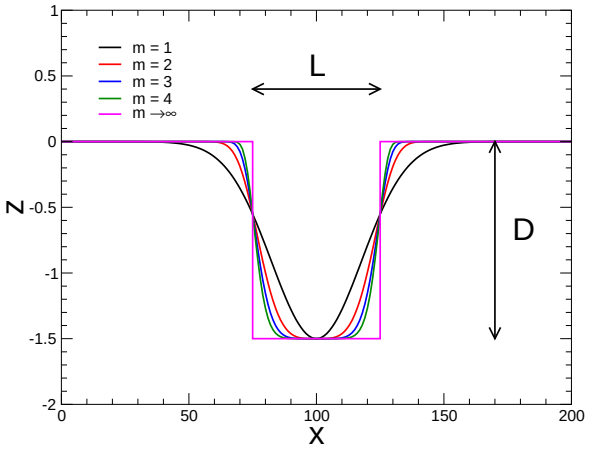

Figure 2: Sketch of the wall shape for several values of the geometrical parameter m in the case of an indentation. The rectangular case can be considered the limiting case when $m \to \infty$.

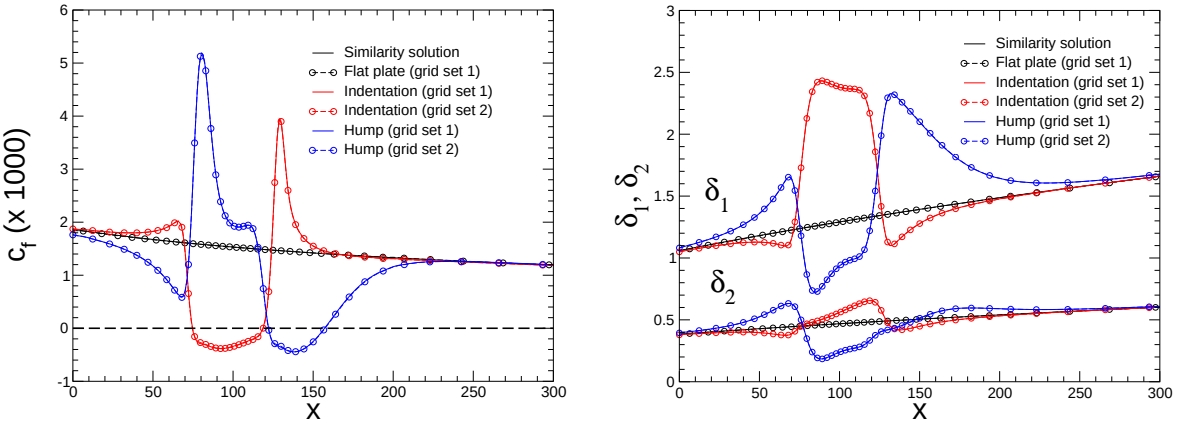

Figure 3: Skin-friction coefficient c_f (left) and boundary-layer displacement thickness δ_1 and momentum thickness δ_2 (right). In the case of indentations and humps, the examples plotted are for $m = 3$. Negative values below the dashed line $c_f = 0$ indicate the position of the recirculation bubbles.

In order to guarantee the grid independence of the basic flow results, two set of grids were considered for all possible humps/indentations. In the second set of grids, both the domain size was extended and the grid resolution in the vicinity of the surface irregularity was increased (compared to the first set of grids). For both sets, inflow was imposed at x = -584, i.e. upstream of the leading edge. In the first sets, the outflow was set at x = 400 and the upper boundary was imposed at $z = 400$. For the second set, these boundaries were extended up to $x = 500$ and $z = 500$ for outflow and upper edge, respectively. In the subdomain $(x, z) \in [0, 200] \cup [0, 6]$, where the surface irregularity is placed, the first set of grids used 120 points in x-direction and 100 points in normal direction. In the second set of grids, these numbers were increased up to 150 points in x-direction, and 130 points in normal direction. For comparison, the distribution of skin-friction coefficient c_f, boundary-layer displacement thickness δ_1 and boundary-layer momentum thickness δ_2 were evaluated for each set of grids. Definition of c_f, δ_1 and δ_2 can be found, *e.g.*

in Schlichting [6]. For all cases results from the two sets of grids are almost identical. This indicates that even the first set of grids is fine enough and does not show any grid influence anymore. As an example, Figure 3 shows the comparison for the results using the two sets of grids in the case of $m = 3$ (both hump and indentation), and also the case of the flat plate computed with TAU compared with the corresponding flat plate similarity solution. Finally, grids from the first set were used for stability analysis.

Figures 4 and 5 reproduce the contours of the streamwise velocity component of the steady laminar two-dimensional flow on a flat plate in the presence of a hump (figure 4) or an indentation (figure 5) for all cases considered in the present paper. The velocity $\bar{u}$ is made nondimensional with U_∞. It is clearly visible that the length and height of the recirculation bubbles increase when the humps/indentations tend to a rectangular shape (i.e. increasing the value of m). The stability analysis performed in the following section will describe the influence of the parameter m on the development of Tollmien-Schlichting (TS) waves along the plate.

3.2 Stability analysis

The stability analysis will be restricted to the spatial development of two-dimensional TS waves. The non-dimensional frequency F is defined as

$$F = 2\pi f \frac{\mu_\infty}{\rho_\infty U_\infty^2} \times 10^6 \tag{13}$$

where f is the physical frequency of the disturbances. In the case of a flat plate without any surface irregularity, the stability analysis has been done using PSE, and it reveals that TS waves of non-dimensional frequencies in the range $F \in [108.6, 217.2]$ produce the highest n-factor curves in the domain $x \in [0, 350]$. When a surface irregularity is present (hump or indentation), the multi-zonal approach is applied (see section 2.2). This approach has been already validated against DNS computations for the stability analysis of 2D TS waves over a flat plate in the presence of a smooth hump (see the work of Franco & Hein [2]). In the multi-zonal framework, computations using PSE have been done up to the section $x = 50$. In this region $x \in [0, 50]$, the presence of the indentation may alter the local pressure distribution with respect to the flat plate case, but due to the small curvature of the hump/indentation and the absence of a recirculation bubble it can be assumed that the PSE approach is valid. In the region $x \in [50, 185]$ the rapid change of the wall geometry and the presence of the recirculation bubble provoke that the changes of any basic flow quantity $\bar{q}$ in x-direction are presumably not small, and therefore the assumptions made in PSE are questionable. Here, the AHLNS methodology is applied. Finally, at some distance of the surface irregularity, in the domain $x \in [185, 350]$, the flow field tends to recover the flat plate solution, and again the PSE approach can be used. To illustrate this procedure, Figure 6 shows the computed n-factor curves for several frequencies[1] in the case of a hump and an indentation (both for $m = 4$). In these curves, the dashed lines indicate PSE computations while solid lines represent AHLNS simulations.

[1]For simplicity in the figures, only few frequencies of the complete stability analysis are depicted.

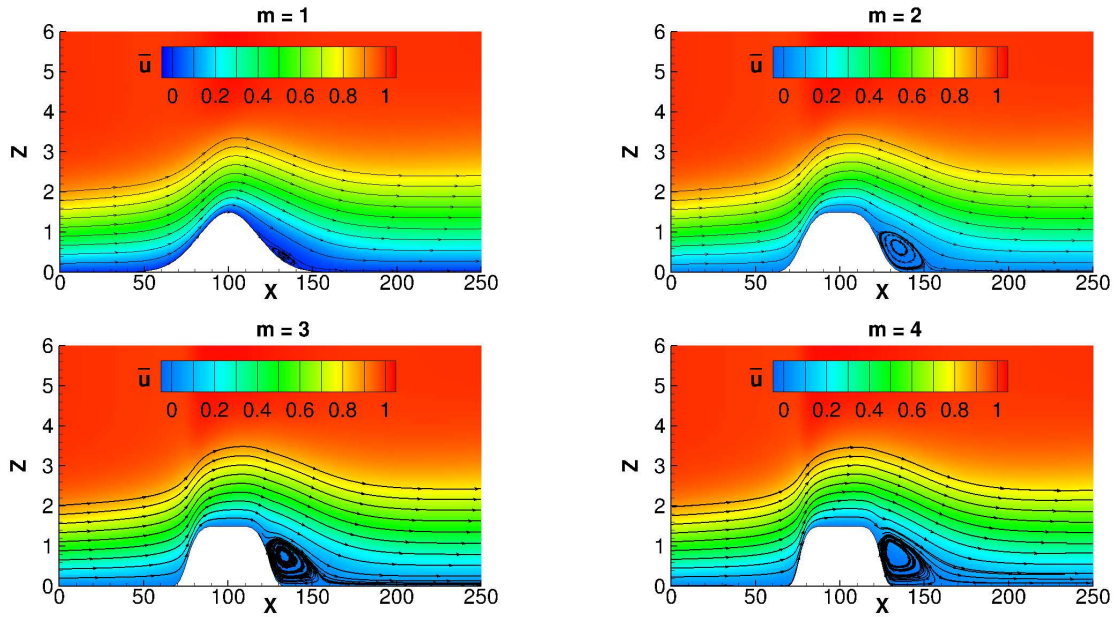

Figure 4: Contours of horizontal velocity component $\bar{u}$ and streamlines for a flat plate in the presence of a hump (m = 1,2,3,4). Velocity contours are made nondimensional with U_∞. Axes not to scale.

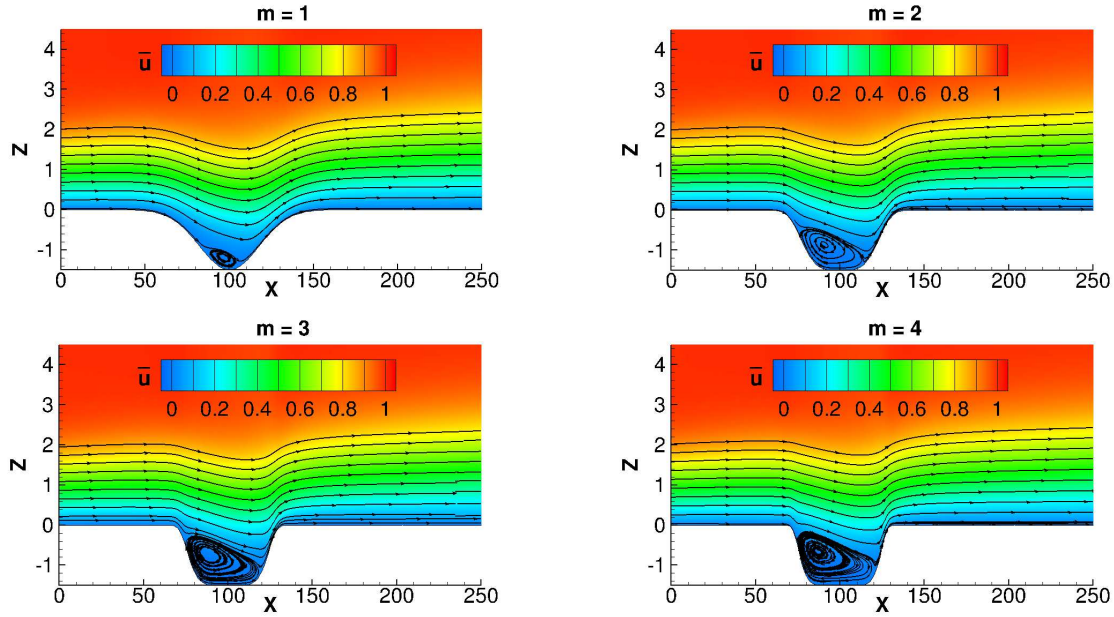

Figure 5: Contours of horizontal velocity component $\bar{u}$ and streamlines for a flat plate in the presence of an indentation (m = 1,2,3,4). Velocity contours are made nondimensional with U_∞. Axes not to scale.

3.2.1 Grid refinements

In order to assure that AHLNS results are grid-independent, 5 grids were tested, with an increasing grid resolution from 111x60 to 191x140 points in the AHLNS domain $x \in [50, 185]$, which is splitted into two subdomains. In the region directly around

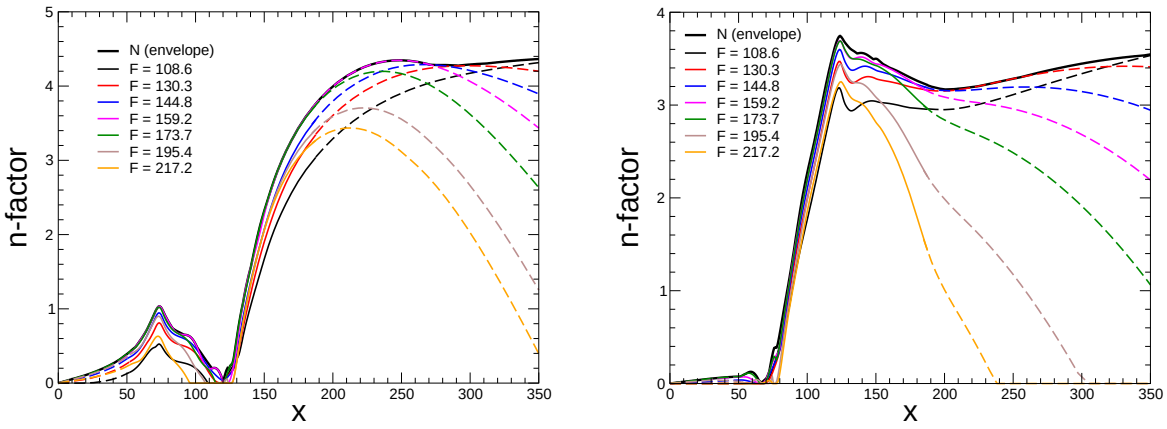

Figure 6: n-factor curves for certain frequencies in the case of a hump (left) and an indentation (right) (both for $m = 4$). Based on multi-zonal approach, solid lines represent AHLNS computations, while dashed lines correspond to PSE computations.

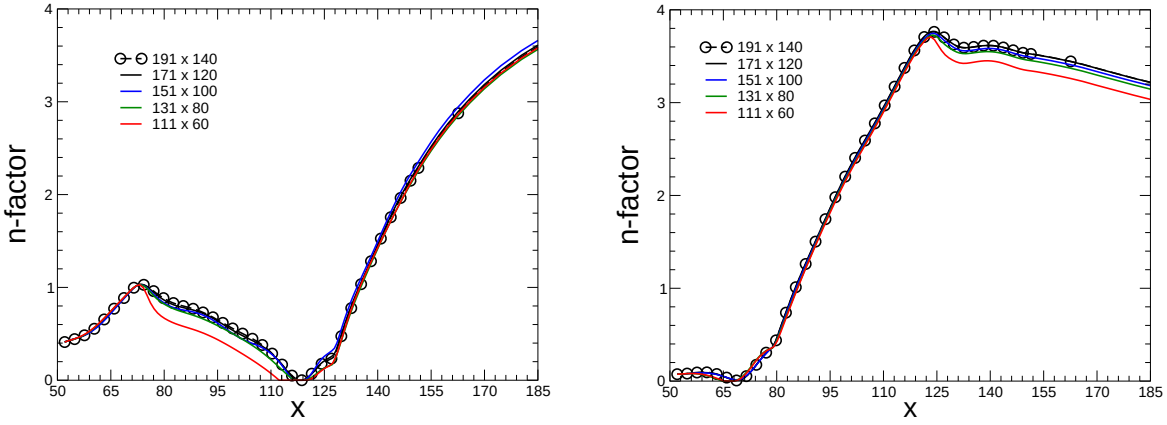

Figure 7: Grid-convergence study for several grid points (n_x, n_z). The evolution of a TS wave of frequency $F = 162.9$ along a hump (left) and an indentation (right) is considered. In both cases $m = 4$.

the hump/indentation $x \in [50, 150]$ grids are equally spaced in x-direction. However, in the domain $x \in [150, 185]$ the grid spacing in x-direction is progressively increased in streamwise direction in order to match with subsequent PSE grid-size requirements (see section 1). In z-direction, all grids are gradually stretched with increasing distance to the wall. In the grid convergence study, solely the number of points (n_x, n_z) was changed. The study was done for the case of $m = 4$, and the evolution of a TS wave of frequency $F = 162.9$ was analyzed. Figure 7 shows that grid convergence was achieved by using a grid with $(n_x, n_z) = (171, 120)$ points in both cases (hump and indentation).

3.2.2 N-factor envelope curves

As it was explained in section 2.3, the N-factor curve is defined as the envelope of the n-factor curves. In the domain $x \in [0, 350]$, TS waves of frequencies in the range $F \in [108.6, 217.2]$ produce the highest n-factor curves for humps and indentations. This

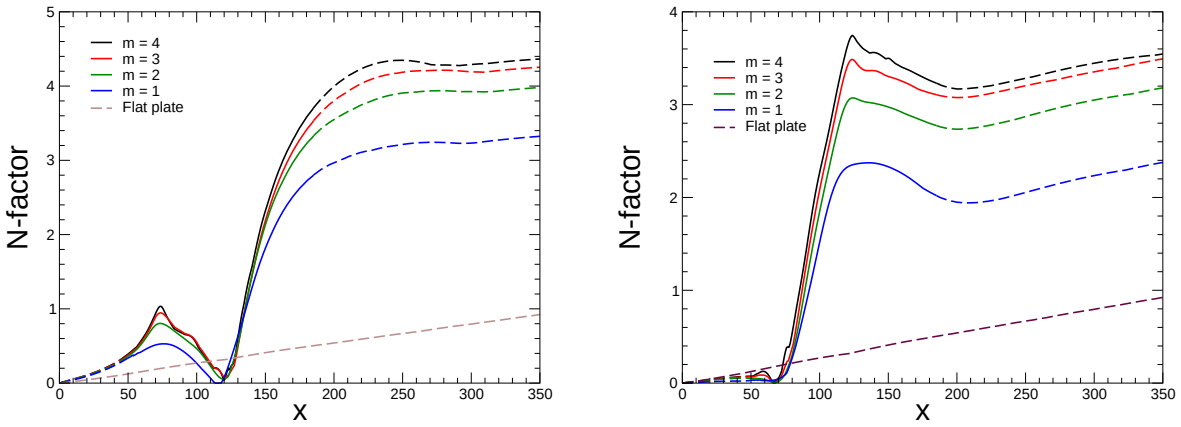

Figure 8: N-factor curve (envelope) in the case of humps (left) and indentations (right) for various values of the geometrical parameter m. Based on multi-zonal approach, solid lines represent AHLNS computations, while dashed lines correspond to PSE computations.

range of frequencies is identical to the case of the flat plate. Therefore, the presence of a hump/indentation simply increases the amplification of the TS waves, but it does not introduce any noticeable shift in the frequency range of the TS waves that contribute to the N-factor envelope in the considered domain. Figure 8 (left) indicates that the presence of a hump introduces a local adverse pressure gradient upstream of the hump that destabilizes the TS waves. Above the hump, there is a local favorable pressure gradient that stabilizes the TS waves around the center of the hump ($x = x_c$). Downstream of the hump, when the TS waves reach the recirculation bubble, there is a rapid increase in the amplitude of the disturbances. Finally, at a certain distance from the hump ($x > 250$), the growth rate of the TS waves recovers the flat plate solution.

In the case of an indentation (Figure 8 - right), the local acceleration of the flow before reaching the recirculation bubble ($x \approx 65$) explains the small decrease in the N-factor curves. This effect is followed by a rapid increase in N-factor due to the presence of the bubble, similar to the effect already seen in the case of the hump. The appearance of a peak in the curves at $x \approx 120$ could be due to a local deceleration of the basic flow. This peak occurs more pronounced when the geometrical parameter m is increased. Perraud and Séraudie noticed a similar N-factor peak also in the case of rectangular forward-facing steps (see [7]), and concluded that this peak could cause an earlier transition in certain cases. Finally, at some distance from the indentation ($x > 200$), the growth rate of the TS waves recovers the flat plate solution. Overall, the presence of a hump/indentation on a flat plate increases significatively the amplitude of the TS waves. In the cases considered in this paper, where the height/depth D and width L of the surface irregularity are fixed, the rise in N-factor depends on the shape of the irregularity itself through the geometrical parameter m. Therefore, it seems reasonable to define a ΔN function that relates the increment of the N-factor envelopes with the geometrical parameter m. The ΔN-factor is defined as

$$\Delta N\left(x, m\right) = N\left(x, m\right) - N_{smooth}\left(x\right), \tag{14}$$

where $N\left(x, m\right)$ represents the value of the N-factor curve for a given value of m at certain

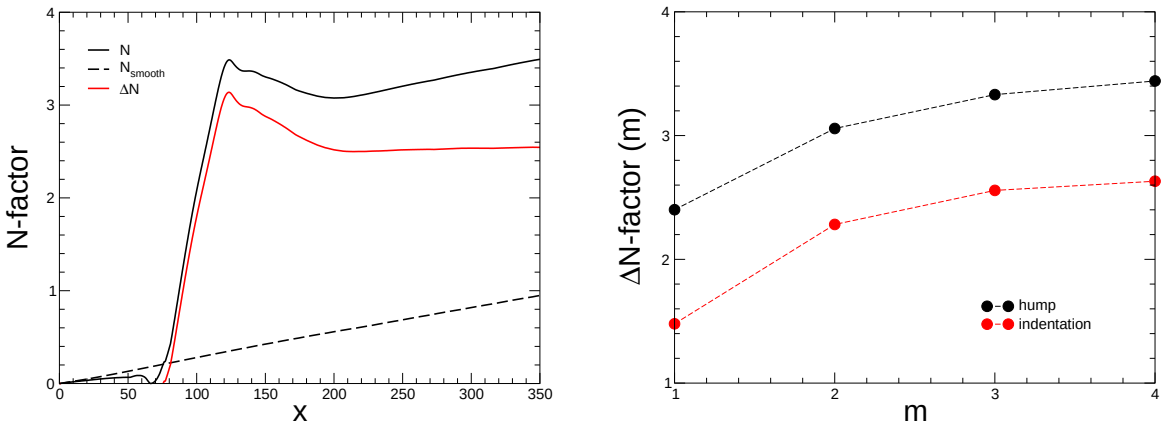

Figure 9: ΔN-factor definition for an indentation with $m = 3$ (left) and ΔN-factor as function of the geometrical parameter m (right).

x location, and $N_{smooth}\,(x)$ is the value of the N-factor envelope computed for the flat plate case. Due to the localized effect of the surface irregularity, the growth rate of the TS waves recovers the flat plate solution and the value of ΔN does no longer depend on the x-location, as it is shown in Figure 9 (left). Consequently, at some distance downstream of the surface irregularity, it is reasonable to assume $\Delta N\,(x, m) \approx \Delta N\,(m)$. If this procedure is repeated for the rest of humps/indentations, it is possible to relate the value of ΔN with m, as it is shown in Figure 9 (right). This figure suggests that the value of $\Delta N\,(m)$ tends to converge to a constant value providing that the value of m is sufficiently increased (for both humps and indentations). This indicates that, for stability analysis purposes, the effect of a particular rectangular hump/indentation could be qualitatively estimated from the effect caused by an equivalent smooth hump/indentation of the same height/depth and width as long as the geometrical parameter m is sufficiently large.

4 CONCLUSIONS

The stability analysis of two-dimensional Tollmien-Schlichting waves over a flat plate in the presence of smooth humps/indentations has been described in this paper. The height/depth and width were fixed, and the shape of the surface irregularity was systematically changed through a geometrical parameter m. It was shown that the presence of humps/indentations leads to a significant rise of the amplitude of the TS waves when the shape of the hump/indentation tends to be rectangular, i.e. increasing the value of m. Moreover, there was no noticeable shift in the frequency range of the TS waves that contribute to the N-factor envelope compared with the flat plate case.

It was shown that, at some distance downstream of the hump/indentation, the ΔN-factor, defined as the difference in N-factor between the surface with hump/indentation with respect to the flat plate case, was uniquely a function of the shape of the irregularity, i.e. m. The simulations presented in this paper suggest that, above certain values of m the corresponding ΔN-factor tends to reach a constant value. This would indicate that, in order to perform a stability analysis of a rectangular hump/indentation, a qualitative estimation could be provided by an equivalent smooth hump/indentation of identical

height/depth and width, as long as the geometrical parameter m is sufficiently large.

5 ACKNOWLEDGMENTS

Authors would like to thank Alexander Theiss (DLR) for providing the Matlab script that extracts data from Tecplot files. Discussions with Jesús Garicano-Mena (UPM) are also gratefully acknowledged. Part of this work was supported by the European project NACOR (Grant Agreement no. CS2-AIR-GAM-2014-2015-01).

REFERENCES

[1] J. Garicano-Mena, E. Ferrer, S. Sanvido and E. Valero. *A stability analysis of the compressible boundary layer flow over indented surfaces*. Computers & Fluids, Vol. **160**, pp. 14–25, 2018.

[2] J. A. Franco and S. Hein. *Adaptive Harmonic Linearized Navier-Stokes equations used for boundary-layer instability analysis in the presence of large streamwise gradients*. AIAA Aerospace Sciences Meeting, AIAA paper 2018-1548, 2018.

[3] Y. Guo, M. Malik, and C. L. Chang. *A solution adaptive approach for computation of linear waves*. AIAA 13th Computational Fluid Dynamics Conference, AIAA paper 1997-2072, 1997.

[4] D. Arnal. *Boundary layer transition: Predictions based on linear theory*. AGARD report 793 - Progress in Transition Modelling, AGARD, 1994.

[5] *TAU-Code User Guide*. V. 2017.1.0.

[6] H. Schlichting. *Boundary-layer theory*. McGraw-Hill, 6th Ed., 1968.

[7] J. Perraud and A. Séraudie. *Effects of steps and gaps on 2D and 3D transition*. ECCOMAS 2000. Barcelona, 11-14 September 2000.

[8] J. P. Nenni and G. L. Gluyas. *Aerodynamic design and analysis of an LFC surface*. Astronautic and Aeronautics, pp. 52-57, 1966.

[9] A. Woerner, U. Rist and S. Wagner. *Humps/Steps influence on stability characteristics of two-dimensional laminar boundary layer*. AIAA Journal, Vol. 41, No. 2, pp. 192-197, 2003.

[10] A. V. Dovgal and V. V. Kozlov. *Hydrodynamic instability and receptivity of small scale separation regions*. Laminar-Turbulent Transition. Proceedings of the IUTAM Symposium, pp. 523-531, 1990.

[11] D. Park and S. O. Park. *Linear and non-linear stability analysis of incompressible boundary layer over a two-dimensional hump*. Computers & Fluids, Vol. **73**, pp. 80–96, 2013.